



# Fast synthesis and formation mechanism of $\gamma$ -MnO<sub>2</sub> hollow nanospheres for aerobic oxidation of alcohols

Xiaobo Fu<sup>a,b</sup>, Jiyun Feng<sup>a,\*</sup>, Huang Wang<sup>a,b</sup>, Ka Ming Ng<sup>a,b</sup>

<sup>a</sup> Nano and Advanced Materials Institute Limited, Clear Water Bay, Hong Kong

<sup>b</sup> Department of Chemical and Biomolecular Engineering, Hong Kong University of Science and Technology, Clear Water Bay, Hong Kong

## ARTICLE INFO

### Article history:

Received 18 November 2009

Received in revised form 24 February 2010

Accepted 18 May 2010

Available online 25 May 2010

### Keywords:

A. Nanostructures

A. Oxides

B. Crystal growth

D. Catalytic properties

## ABSTRACT

$\gamma$ -MnO<sub>2</sub> hollow nanospheres of about 300–800 nm in size have been synthesized by a fast 1-h 2-step process in the presence of an excess amount of Mn<sup>2+</sup> in aqueous solution without using any templates, hydrothermal processes and catalytic routes. The evolution of morphologies evidenced that the fast formation mechanism of the  $\gamma$ -MnO<sub>2</sub> hollow nanospheres in the presence of the excess amount of Mn<sup>2+</sup> in solution followed the “Ostward ripening” process. The as-synthesized  $\gamma$ -MnO<sub>2</sub> hollow nanospheres showed high catalytic activity and selectivity in aerobic oxidation of various alcohols which was attributed to their hollow nature and larger BET specific surface area.

© 2010 Elsevier Ltd. All rights reserved.

## 1. Introduction

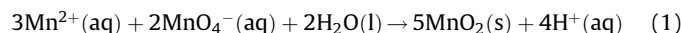
The synthesis of metal oxides with controlled morphology has shown profound significance in physical chemistry [1,2]. Recently, manganese dioxide (MnO<sub>2</sub>) hollow structures have become attractive owing to their specific physical and chemical properties, such as large surface area, low density and good permeability [3–8]. Three methods have been developed to synthesize MnO<sub>2</sub> hollow structures including template based methods, hydrothermal processes, and catalytic routes. For template method [6,9,10], the removal of templates by acid or base etching, or calcination, may damage the desired hollow structures, and the subsequent purification procedures could significantly increase the costs. For hydrothermal processes [8,11–13], even though the hollow structures can form with regular morphology, the operating conditions are severe and it is difficult to be produced on a large scale. For the catalytic route, Xie and co-workers [3] used a solution based catalytic method to fabricate different  $\alpha$ -MnO<sub>2</sub> hollow structures. Their catalytic route cast new light on the development of new superstructures. However, the time for synthesizing the MnO<sub>2</sub> hollow structures by those methods is very long. Thus, in spite of many methods reported for synthesizing MnO<sub>2</sub> hollow structures, a fast and simple method without using any templates, catalysts, and hydrothermal processes, has not been fully developed. Developing such a method is expected to have both academic and industrial significance.

Usually, the MnO<sub>2</sub> crystallization proceeds through two steps: a disordered [14] or layered [15,16] manganese oxide precursor is formed, followed by an aging process to form the final product with ordered structure. The structure and the morphology of the final product are dependent on the aging process. In addition, a high aging temperature can accelerate the crystallization process of MnO<sub>2</sub> in solution [17]. Based on these findings, herein, we report a fast 1-h 2-step process for synthesizing novel  $\gamma$ -MnO<sub>2</sub> hollow nanospheres in solution without using any templates, catalysts and hydrothermal processes. This process consisted of the reaction between MnSO<sub>4</sub> and KMnO<sub>4</sub> in aqueous solution in the presence of an excess amount of Mn<sup>2+</sup> at room temperature for 0.5 h to obtain a solid precursor, followed by an aging of the solution at 60 °C for another 0.5 h to obtain the  $\gamma$ -MnO<sub>2</sub> hollow nanospheres. The as-synthesized  $\gamma$ -MnO<sub>2</sub> hollow nanospheres were characterized by powder X-ray diffraction (XRD), scanning electron microscopy (SEM), transmission electron microscopy (TEM), and BET analyses. Their fast formation mechanism at 60 °C in solution was discussed, and their catalytic activities were also evaluated in the aerobic oxidation of various alcohols.

## 2. Experiments

### 2.1. Synthesis

Our synthesis is based on the following reaction between MnSO<sub>4</sub> and KMnO<sub>4</sub> in aqueous solution.



\* Corresponding author. Fax: +852 23588113.

E-mail addresses: [kejyfeng@ust.hk](mailto:kejyfeng@ust.hk), [kejyfeng@gmail.com](mailto:kejyfeng@gmail.com) (J. Feng).

In the synthesis, 8.50 g analytical grade  $\text{MnSO}_4 \cdot \text{H}_2\text{O}$  and 3.43 g analytical grade  $\text{KMnO}_4$  powders were mixed together ( $\text{MnSO}_4/\text{KMnO}_4$  mole ratio = 2.3), and ground to fine powder in an automatic mortar at room temperature for 1 h. Then, the mixed powder was transferred to 200 mL distilled water in a beaker under continuous stirring. After that, 100 mL of 1 M  $\text{H}_2\text{SO}_4$  solution was immediately added to the beaker to accelerate the reaction rate and remove potassium ions. The solution was firstly kept at room temperature with vigorous stirring for 0.5 h to obtain the precursor. Then, the solution was transferred to a water bath at  $60^\circ\text{C}$  with a condenser for another 0.5 h with vigorous stirring, which was an aging process to accelerate the crystallization of the precursor and form the  $\text{MnO}_2$  hollow nanospheres. Finally, the precipitates were filtered and rinsed with distilled water and ethanol to remove any chemical species possibly remaining in the final product. The resultant product was then dried in an oven at  $70^\circ\text{C}$  overnight. Some control experiments were also conducted which will be discussed later.

## 2.2. Characterization

Phase identification and structure analysis of the precursor and the as-synthesized product were performed on a PANalytical X'pert Pro X-ray Diffractometer equipped with  $\text{Cu K}\alpha$  radiation ( $\lambda = 1.54178 \text{ \AA}$ ), operating at 40 kV and 40 mA. The morphologies of the two products were studied by a field emission scanning electron microscope (FESEM, JEOL JSM-6700F) with an accelerating voltage of 5 kV and a transmission electron microscope (JEOL-2010F) with an accelerating voltage of 200 kV, equipped with a Bruker Energy Dispersive Spectrometer (EDS). The BET specific surface area was determined by  $\text{N}_2$  adsorption at 77 K using a Micromeritics ASAP 2000 system after the sample was degassed in vacuum at  $130^\circ\text{C}$  overnight.

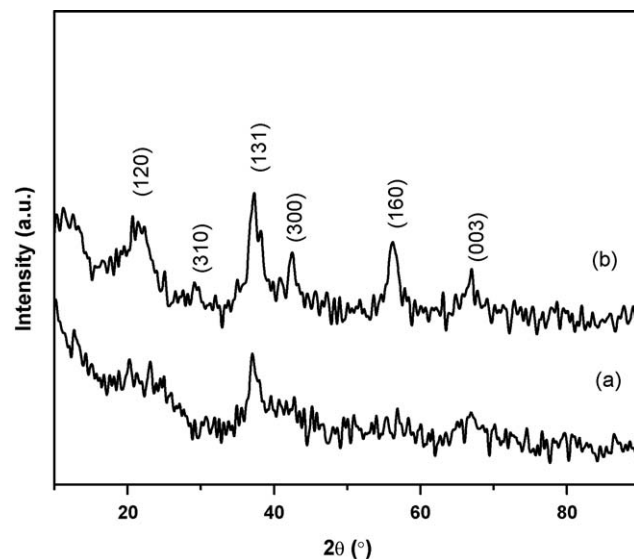


Fig. 1. XRD patterns for (a) the precursor obtained at solution reaction for 0.5 h at room temperature, and (b) the as-synthesized product.

## 2.3. Evaluation of catalytic activity

For a typical procedure of the alcohol oxidation, toluene (10 mL) and the substrate (1 mmol) were first added to a 25 mL round-bottomed flask containing 0.05 g catalyst. The mixture was then stirred under reflux at  $110^\circ\text{C}$  with air bubbling, which was controlled by a mass flow controller with a flow rate of 10 mL/min. After reaction for 4 h, the reaction mixture was cooled down to room temperature. The filtrate was carefully analyzed using a gas chromatography/mass spectrometry (GC/MS) fitted with a HP-1MS column.

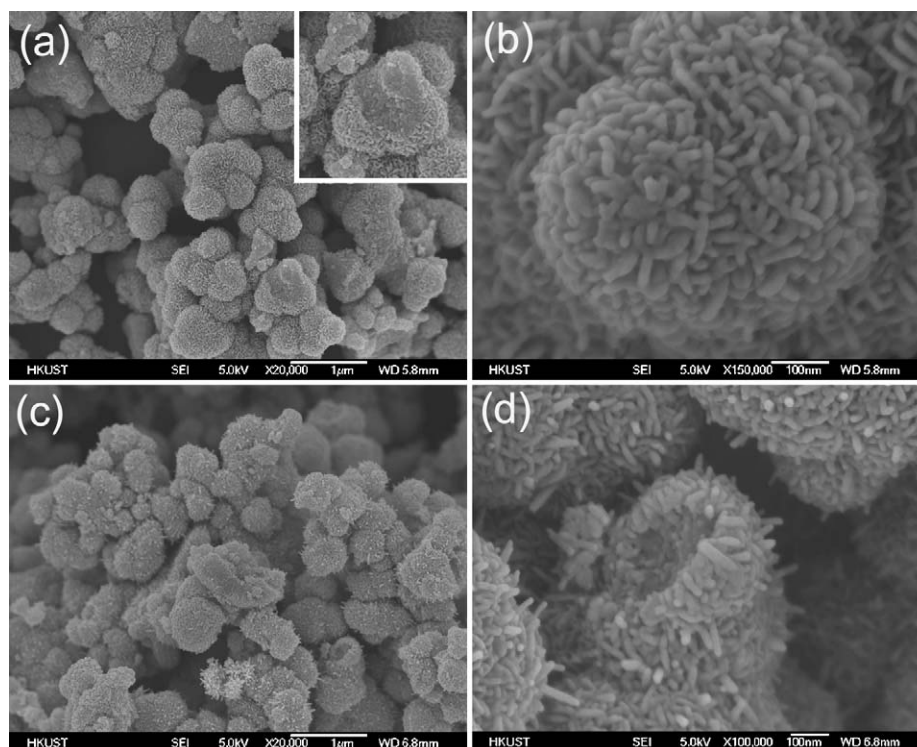


Fig. 2. SEM images of the precursor obtained at solution reaction for 0.5 h at room temperature (a and b) and the as-synthesized product (c and d) (the inset is a higher magnification of the solid nanosphere).

### 3. Results and discussion

Fig. 1 shows the XRD patterns of the precursor and the as-synthesized product, indicating that the precursor was poorly ordered while the as-synthesized product was in  $\gamma$ -MnO<sub>2</sub> crystalline phase because all its major diffraction peaks can be assigned to the orthorhombic phase of  $\gamma$ -MnO<sub>2</sub> with lattice constants  $a = 6.36 \text{ \AA}$ ,  $b = 10.15 \text{ \AA}$  and  $c = 4.09 \text{ \AA}$  (JCPDS 14-644). The XRD results also reveal that  $\gamma$ -MnO<sub>2</sub> crystalline phase formed quickly from the poorly ordered precursor within 0.5 h aging at 60 °C in the presence of the excess amount of MnSO<sub>4</sub> in solution. In addition, the BET specific surface area of the as-synthesized product was determined to be  $158 \text{ m}^2 \text{ g}^{-1}$ . The SEM image in Fig. 2a shows that the precursor consisted of aggregated nanospheres with diameter about 300–800 nm. A broken nanosphere in the image (as shown in the inset of Fig. 2a) reveals that these nanospheres were solid. The SEM image in Fig. 2b depicts that many nanorods with diameter about 10 nm and length about

50 nm emerged on the surface of the solid nanosphere. Fig. 2c shows that the overall morphology of the as-synthesized product was similar to that of the precursor. However, the length of the nanorods increased from about 50 nm to about 100 nm, implying that the length of the nanorods increased quickly at 60 °C within 0.5 h in solution in the presence of excess amount of MnSO<sub>4</sub>. In addition, the SEM image of a broken nanosphere in Fig. 2d reveals that the nanospheres were hollow. The morphology of the hollow nanospheres is significantly different from that of the hollow urchin structure consisting of long and uniform fibers pointing outward reported by other researchers [3,8,10,13]. Elemental analysis indicated that only trace amount (less than 0.1%) of K<sup>+</sup> was detected in both the precursor and the as-synthesized product.

The TEM images in Fig. 3a and b reveal that the precursor was made of aggregated solid nanospheres. On the contrary, the dark-bright contrast between the boundary and the center of the nanospheres in Fig. 3c and d strongly confirms that the as-synthesized product consisted of aggregated hollow nanospheres.

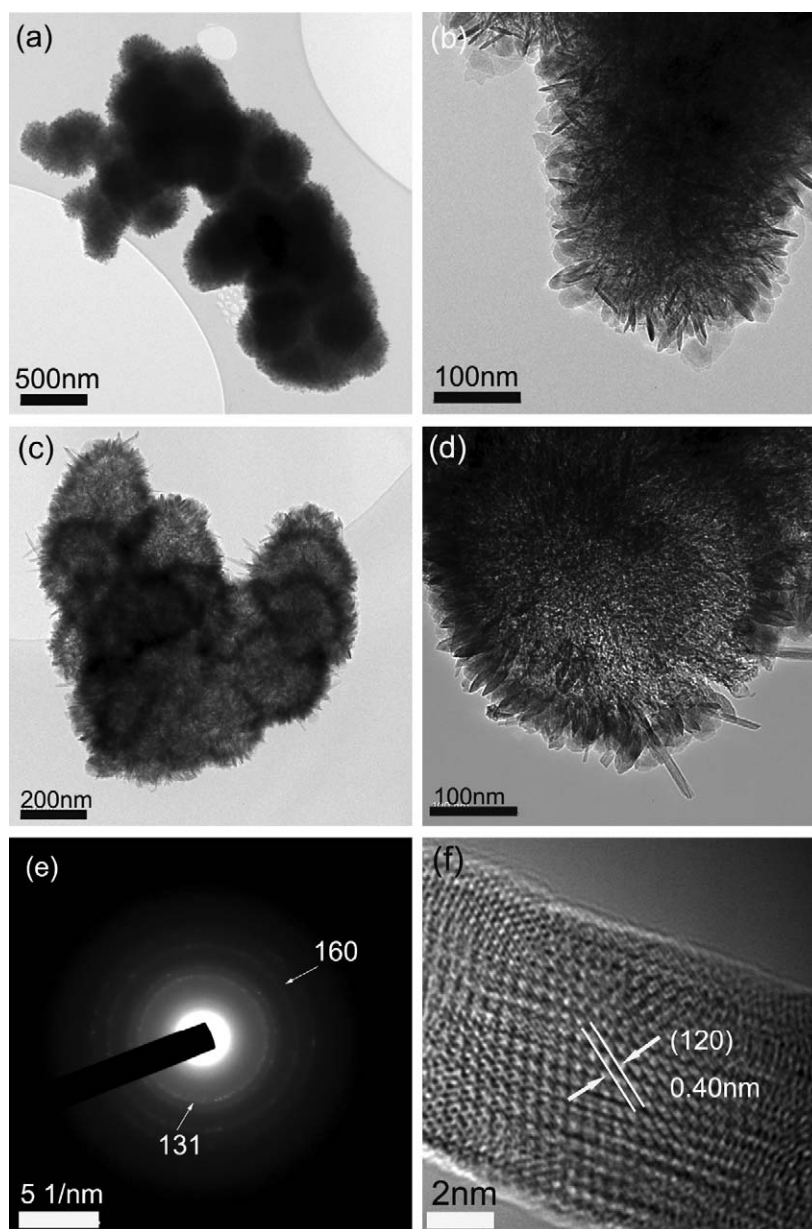
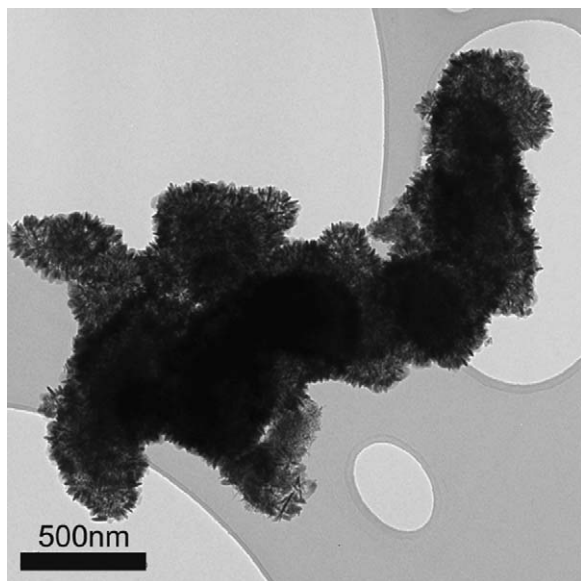


Fig. 3. TEM images of the precursor obtained at solution reaction for 0.5 h at room temperature (a and b) and the as-synthesized product (c and d), SAED pattern (e) and HRTEM image (f) of the s-synthesized product.



**Fig. 4.** A TEM image of the product obtained by 0.5 h room temperature reaction followed by another 2.5 h aging at room temperature.

The characteristic distances of the  $\gamma$ -MnO<sub>2</sub> hollow nanospheres, even though without preferred orientation of the crystallites, could be seen, which is shown in the SAED pattern in Fig. 3e. Fig. 3f is a HRTEM image of a single nanorod located at a hollow structure, confirming that the nanorod is crystalline; the lattice spacing of 0.40 nm is consistent with that of the  $\gamma$ -MnO<sub>2</sub> (1 2 0) plane. Therefore, both SEM and TEM images confirm that the novel hollow nanospheres could be obtained via 0.5 h reaction in solution at room temperature followed by another 0.5 h aging at 60 °C in solution in the presence of an excess amount of MnSO<sub>4</sub>. In other words, a higher temperature in the aging process led to a fast formation of the  $\gamma$ -MnO<sub>2</sub> hollow nanospheres. In order to verify this, a control experiment was conducted. After 0.5 h reaction at room temperature, the reaction solution was still kept at room temperature, even though the aging time was extended to 2.5 h, only solid nanospheres were obtained, as shown in Fig. 4.

Many efforts have been made to synthesize MnO<sub>2</sub> materials in aqueous acidic solutions under reflux and with varying oxidizing agents (KMnO<sub>4</sub>) concentrations. However, to the best of our knowledge, no intensive study had been made on the varying the MnSO<sub>4</sub> concentrations to form the  $\gamma$ -MnO<sub>2</sub> hollow nanospheres. Our control experimental results indicate that the  $\gamma$ -MnO<sub>2</sub> hollow nanospheres could not be formed when the mole ratio of the MnSO<sub>4</sub> to KMnO<sub>4</sub> was less than 2.3 (the stoichiometric ratio of the MnSO<sub>4</sub> to KMnO<sub>4</sub> is 1.5), demonstrating that the excess amount of the MnSO<sub>4</sub> in solution played an important role in the formation of the hollow nanospheres and the grinding process was not a key step. However, Mn<sup>2+</sup> or SO<sub>4</sub><sup>2-</sup> may be responsible for the formation of the  $\gamma$ -MnO<sub>2</sub> hollow nanospheres, but which one plays the real role had to be investigated. Thus, a control experiment was conducted, in which MnSO<sub>4</sub> and KMnO<sub>4</sub> were used as the starting materials to react firstly in stoichiometric ratio, then Mn(AC)<sub>2</sub> was added to the system to replace the corresponding excess amount of MnSO<sub>4</sub> in the synthesis of the  $\gamma$ -MnO<sub>2</sub> hollow nanospheres. We found that the  $\gamma$ -MnO<sub>2</sub> hollow nanospheres still formed, as shown in Fig. 5a. In another control experiment, ZnSO<sub>4</sub> was used to replace the corresponding excess amount of MnSO<sub>4</sub> to verify the function of the SO<sub>4</sub><sup>2-</sup>. However, only  $\gamma$ -MnO<sub>2</sub> solid nanospheres formed, as shown in Fig. 5b. Therefore, it is clearly revealed that the excess amount of the Mn<sup>2+</sup> in solution was responsible for the formation of the  $\gamma$ -MnO<sub>2</sub>

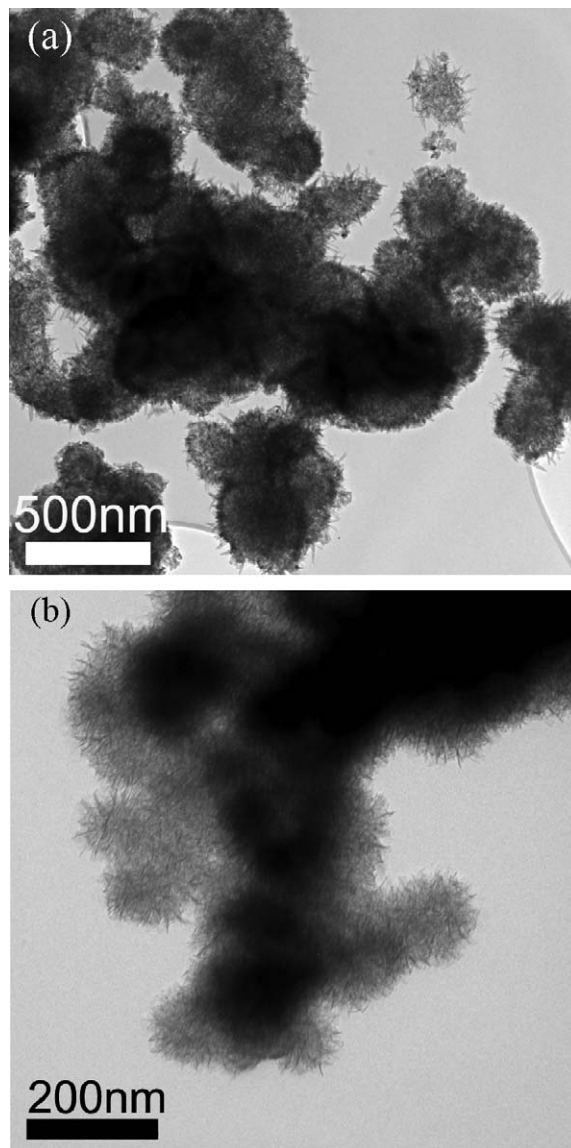


**Fig. 5.** TEM images of the product obtained by using Mn(AC)<sub>2</sub> (a) or ZnSO<sub>4</sub> (b) to replace the excess amount of MnSO<sub>4</sub> in solution.

hollow nanospheres. At the same time, the weight of the product (about 5.73 g) is larger than the theoretical weight (about 4.72 g) which can be calculated using the reaction between Mn<sup>2+</sup> and MnO<sub>4</sub><sup>-</sup>, implying that a secondary reaction involving the oxidation of the excess amount of Mn<sup>2+</sup> by the oxygen also took place in solution as displayed in Eq. (2).



The MnO<sub>2</sub> generated through this reaction would promote the re-crystallization of the solid nanospheres.

The results above enable us to propose a formation mechanism for the  $\gamma$ -MnO<sub>2</sub> hollow nanospheres in this fast 1-h 2-step process, as shown in Fig. 6. The initial reaction at room temperature between Mn<sup>2+</sup> and MnO<sub>4</sub><sup>-</sup> was too fast to enable orientation between the sheets of MnO<sub>6</sub> octahedron, leading to the formation of poorly ordered solid nanospheres. Then, fast growth of the nuclei occurred. After that, owing to the complete consumption of the KMnO<sub>4</sub>, the system was transformed into a thermodynamically stable state. As the system was in an acidic condition and in the absence of the complexant, it seems that Mn species were

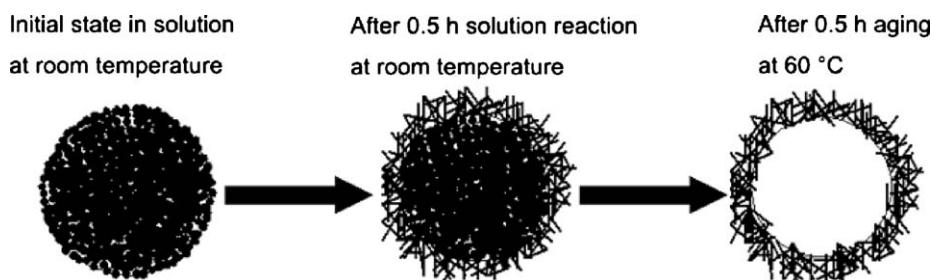


Fig. 6. Schematic illustration of the fast formation mechanism of the  $\gamma$ -MnO<sub>2</sub> hollow nanospheres via an Ostwald ripening process.

favorable to dissolve [17]. Therefore, the early precipitate might not reserve its shape and disordered structure.

Basically, the growth of MnO<sub>2</sub> mainly follows three processes: dissolution-crystallization, oriented attachment and lateral growth [10,17]. In our process, the nanorods were connected by several nanoparticles, as can be clearly seen in Fig. 7. This may be caused by a dissolution-crystallization first, followed by an oriented attachment, which was also observed by Adachi et al. [18,19] and Penn et al. [19]. As the aging process proceeded, the crystallites in the inner core, having higher surface energy than those on the outer surfaces, were easily dissolved in the presence of the excess amount of the Mn<sup>2+</sup> in solution. Then, the outside nanorods served as sites for subsequent crystallization process of the cores, and they grew at the expense of the small crystallites in the cores. The direct evidence for the process is that the size and length of the nanorods increased from about 5 nm and 50 nm to about 10 nm and 100 nm, as mentioned in SEM and TEM characterizations. Finally, an interior cavity gradually formed. However, it should be stressed that the process could hardly happen or need a very long time at room temperature. Because an increased temperature could effectively accelerate the crystallization of MnO<sub>2</sub> in solution as reported by Portehault et al. [17], we accelerated the crystallization of the MnO<sub>2</sub> solid nanospheres by transferring the reaction system from room temperature to 60 °C water bath for aging. Finally, hollow  $\gamma$ -MnO<sub>2</sub> nanospheres quickly formed within 0.5 h aging in solution. All the results demonstrated that the fast formation mechanism of  $\gamma$ -MnO<sub>2</sub> hollow nanospheres at 60 °C in the presence of the excess amount of Mn<sup>2+</sup> in solution followed an Ostwald ripening process, in which the initial formation of tiny crystalline nuclei in a supersaturated medium is followed by crystal growth and the larger crystals grow at the expense of the

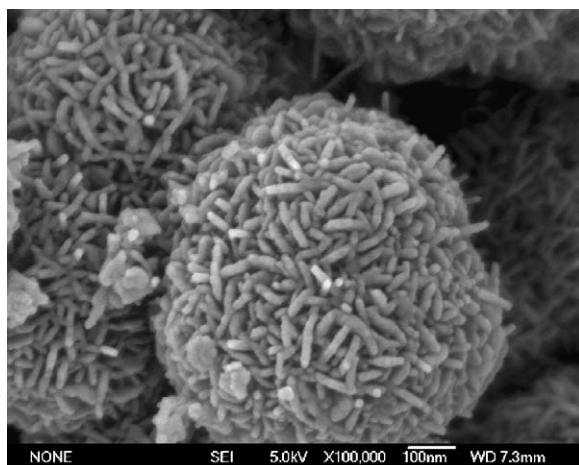


Fig. 7. A high resolution SEM image of the as-synthesized  $\gamma$ -MnO<sub>2</sub> hollow nanospheres.

small crystals because of the energy difference between them [20].

Conventional MnO<sub>2</sub> have been used for allylic and benzylic oxidations, and their catalytic activities depend on the preparations, compositions, crystal structures, and morphologies [21]. The novel  $\gamma$ -MnO<sub>2</sub> hollow nanospheres were used as a catalyst in the aerobic oxidation of various alcohols, and the results are listed in Table 1, indicating that the  $\gamma$ -MnO<sub>2</sub> hollow nanospheres gave excellent conversions and selectivity both for saturated and unsaturated alcohols. Compared with the MnO<sub>2</sub>-OMS reported [21], our  $\gamma$ -MnO<sub>2</sub> hollow nanospheres showed higher catalytic activities and selectivity under identical reaction conditions, which

Table 1

Aerobic oxidation of alcohols using  $\gamma$ -MnO<sub>2</sub> hollow nanospheres as catalysts.

Substrates	Products	Time (h)	Conversion (%)	Selectivity (%)	TON <sup>a</sup>
		4	100	>99	1.73
		4	100	>99	1.73
		4	100	>99	1.73
		4	97	>99	1.73
		4	98	>99	1.68
		4	100	>99	1.73
		4	50	>99	0.87
		4	40	>99	0.69
		4	90	>99	1.56

Reaction conditions: 1 mol cinnamyl alcohol, 10 mL toluene, 0.05 g catalyst, T = 110 °C and pressure = 0.1 MPa; flow rate of air: 10 mL/min.

<sup>a</sup> Turn over number based on substrate per mole MnO<sub>2</sub>.

<sup>b</sup> From Ref. [21].

may be attributed to their hollow nature and larger BET specific surface areas. These results demonstrated that the  $\gamma$ -MnO<sub>2</sub> hollow nanospheres can be used as an efficient catalyst for the aerobic oxidation of alcohols.

#### 4. Conclusions

In summary, this is the first reported synthesis of  $\gamma$ -MnO<sub>2</sub> hollow nanospheres by a 1-h 2-step process without using any templates, catalysts, and hydrothermal processes, which is the shortest reaction time reported in the literature to date. This process consisted of the reaction between MnSO<sub>4</sub> and KMnO<sub>4</sub> in aqueous solution in the presence of an excess amount of Mn<sup>2+</sup> at room temperature for 0.5 h, followed by an aging of the solution at 60 °C for another 0.5 h. The  $\gamma$ -MnO<sub>2</sub> hollow nanospheres with a diameter of about 300–800 nm consisted of nanorods with diameter about 8–10 nm and length about 50–100 nm. The excess amount of the Mn<sup>2+</sup> in solution was found to be the key factor in the formation of the  $\gamma$ -MnO<sub>2</sub> hollow nanospheres. The fast formation mechanism of the  $\gamma$ -MnO<sub>2</sub> hollow nanospheres at 60 °C in the presence of the excess amount of Mn<sup>2+</sup> in solution followed the “Ostward ripening” process. The as-synthesized  $\gamma$ -MnO<sub>2</sub> hollow nanospheres showed high catalytic activity and selectivity in aerobic oxidation of various alcohols because of their larger BET specific surface area. This facile 1-h 2-step synthetic process provides a new perspective of the fast synthesis of  $\gamma$ -MnO<sub>2</sub> hollow nanospheres.

#### References

- [1] H.G. Yang, C.H. Sun, S.Z. Qiao, J. Zou, G. Liu, S.C. Smith, H.M. Cheng, G.Q. Lu, *Nature* 453 (2008) 638.
- [2] H.G. Yang, G. Liu, S.Z. Qiao, C.H. Sun, Y.G. Jin, S.C. Smith, J. Zou, H.M. Cheng, G.Q. Lu, *J. Am. Chem. Soc.* 131 (2009) 4078.
- [3] Z.Q. Li, Y. Ding, Y.J. Xiong, Q. Yang, Y. Xie, *Chem. Commun.* 7 (2005) 918.
- [4] X.F. Shen, Y.S. Ding, J. Liu, J. Cai, K. Laubernds, R.P. Zenger, A. Vasiliev, M. Aindow, S.L. Suib, *Adv. Mater.* 17 (2005) 805.
- [5] B.X. Li, G.X. Rong, Y. Xie, L.F. Huang, C.Q. Feng, *Inorg. Chem.* 45 (2006) 6404.
- [6] J.B. Fei, Y. Cui, X.H. Yan, W. Qi, Y. Yang, K.W. Wang, Q. He, J.B. Li, *Adv. Mater.* 20 (2008) 452.
- [7] J.M. Shin, R. Md Anisur, M.K. Ko, G.H. Im, J.H. Lee, I.S. Lee, *Angew. Chem. Int. Ed.* 48 (2009) 321.
- [8] P. Yu, X. Zhang, D.L. Wang, L. Wang, Y.W. Ma, *Cryst. Growth Des.* 9 (2009) 528.
- [9] X. Wang, Y.D. Li, *Chem. Commun.* 7 (2002) 764.
- [10] N. Wang, Y. Gao, J. Gong, X.Y. Ma, X.L. Zhang, Y.H. Guo, L.Y. Qu, *Eur. J. Inorg. Chem.* 24 (2008) 3827.
- [11] Y.S. Ding, X.F. Shen, S. Gomez, H. Luo, M. Aindow, S.L. Suib, *Adv. Funct. Mater.* 16 (2006) 549.
- [12] W.N. Li, J.K. Yuan, X.F. Shen, S. Gomez-Mower, L.P. Xu, S. Sithambaram, M. Aindow, S.L. Suib, *Adv. Funct. Mater.* 16 (2006) 1247.
- [13] M. Xu, L. Kong, W. Zhou, H. Li, *J. Phys. Chem. C* 111 (2007) 19141.
- [14] J.C. Villegas, L.J. Garces, S. Gomez, J.P. Durand, S.L. Suib, *Chem. Mater.* 17 (2005) 1910.
- [15] X. Wang, Y.D. Li, *Chem. Eur. J.* 9 (2003) 300.
- [16] X.F. Shen, Y.S. Ding, J.C. Hanson, M. Aindow, S.L. Suib, *J. Am. Chem. Soc.* 128 (2006) 4570.
- [17] D. Portehault, S. Cassaignon, E. Baudrin, J.P. Jolivet, *Chem. Mater.* 19 (2007) 5410.
- [18] M. Adachi, Y. Murata, J. Takao, J.T. Jiu, M. Sakamoto, F.M. Wang, *J. Am. Chem. Soc.* 126 (2004) 14943.
- [19] R.L. Penn, J.J. Erbs, D.M. Gulliver, *J. Cryst. Growth* 293 (2006) 1.
- [20] W.Z. Ostwald, *Phys. Chem.* 34 (1900) 495.
- [21] Y.C. Son, V.D. Makwana, A.R. Howell, S.L. Suib, *Angew. Chem. Int. Ed.* 40 (2001) 4280.